iScience

CellPress
OPEN ACCESS

Article

GPCR Genes as Activators of Surface Colonization Pathways in a Model Marine Diatom

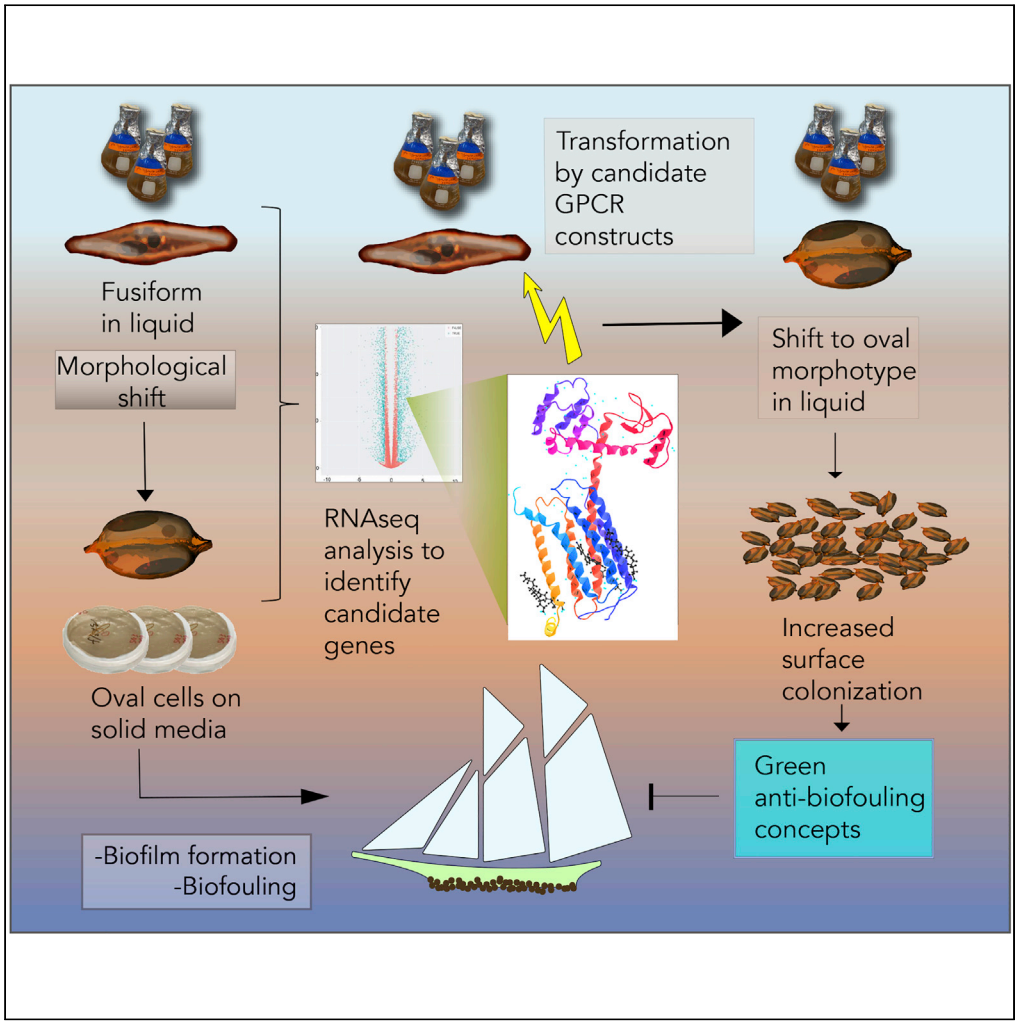

Weiqi Fu, Amphun Chaiboonchoe, Bushra Dohai, ..., Alexandra Mystikou, Sigurdur Brynjolfsson, Kourosh Salehi-Ashtiani

wf21@nyu.edu (W.F.)
ksa3@nyu.edu (K.S.-A.)

HIGHLIGHTS

The model diatom *Phaeodactylum tricornutum* shifts morphology to form biofilms

G-protein-coupled receptors (GPCRs) can modulate diatom surface colonization

GPCR1A expression can induce biofouling morphotype and UV resistance

Identified genes and pathways can serve as targets for anti-biofouling discoveries

Fu et al., iScience *23*, 101424
August 21, 2020
https://doi.org/10.1016/j.isci.2020.101424

iScience

CellPress
OPEN ACCESS

Article

GPCR Genes as Activators of Surface Colonization Pathways in a Model Marine Diatom

Weiqi Fu,[1,2,*] Amphun Chaiboonchoe,[1] Bushra Dohai,[1] Mehar Sultana,[3] Kristos Baffour,[1] Amnah Alzahmi,[3,5] James Weston,[4] Dina Al Khairy,[1] Sarah Daakour,[3] Ashish Jaiswal,[1] David R. Nelson,[3] Alexandra Mystikou,[3] Sigurdur Brynjolfsson,[2] and Kourosh Salehi-Ashtiani[1,3,6,*]

SUMMARY

Surface colonization allows diatoms, a dominant group of phytoplankton in oceans, to adapt to harsh marine environments while mediating biofoulings to human-made underwater facilities. The regulatory pathways underlying diatom surface colonization, which involves morphotype switching in some species, remain mostly unknown. Here, we describe the identification of 61 signaling genes, including G-protein-coupled receptors (GPCRs) and protein kinases, which are differentially regulated during surface colonization in the model diatom species, *Phaeodactylum tricornutum*. We show that the transformation of *P. tricornutum* with constructs expressing individual *GPCR* genes induces cells to adopt the surface colonization morphology. *P. tricornutum* cells transformed to express *GPCR1A* display 30% more resistance to UV light exposure than their non-biofouling wild-type counterparts, consistent with increased silicification of cell walls associated with the oval biofouling morphotype. Our results provide a mechanistic definition of morphological shifts during surface colonization and identify candidate target proteins for the screening of eco-friendly, anti-biofouling molecules.

INTRODUCTION

Diatoms (Bacillariophyta) are the dominant group of microalgae in today's oceans (Benoiston et al., 2017; Mock et al., 2017) and one of the most diverse and ecologically important clades of phytoplankton, contributing up to 20% of the global primary production (Bowler et al., 2008; Levitan et al., 2014; Vardi et al., 2008). Diatoms are recognized as the primary contributor to biofilm formation in marine or underwater environments, a process that leads to biofouling (Bruckner et al., 2011; Callow and Callow, 2011; Dang and Lovell, 2016; Finlay et al., 2013; Garacci et al., 2019; Salta et al., 2013; Vanelslander et al., 2012). Marine biofouling has significant impacts on immersed artificial structures such as ship hulls, aquaculture cage facilities, and seawater handling pipes (Leterme et al., 2016; Salta et al., 2013). Particularly, biofouling on ships increases fuel and maintenance costs significantly (Salta et al., 2013). Conversely, surface colonization and biofilm formation have substantial physiological advantages for microalgae in response to stress conditions and also play important roles in microbial adaptation to fluctuations in marine environments (Dang and Lovell, 2016; Schaum, 2019).

A hallmark of the diatom cell wall is its siliceous structure, called the frustule, which is typically made of silicon dioxide (SiO_2) particles having diameter ranging from 10 to 100 nm (De Tommasi et al., 2017; Vardi et al., 2008). Unlike other known diatoms, the diatom *Phaeodactylum tricornutum*, can grow in the absence of silicon and exists in different morphotypes such as fusiform, oval, and triradiate cell forms. Among these forms, only the oval cells make silicified frustules (De Martino et al., 2011; Lewin et al., 1958). The oval cell forms only become dominant in *P. tricornutum* culture population in response to environmental stress and during biofilm formation on solid surfaces in which cells form aggregates (De Martino et al., 2011; Francius et al., 2008). Silica plays an essential role in cell metabolism in *P. tricornutum* when it makes morphology shift from fusiform to oval in response to environmental stress. To date, *P. tricornutum* is the only known diatom species that can grow without silicon, and this feature makes it an ideal model to study cell morphology and how related molecular regulation underlies adaptive capability in marine environments. Although different strains/accessions of *P. tricornutum* differ in phenotypes as well as genotypes

[1]Laboratory of Algal, Systems, and Synthetic Biology (LASSB), Division of Science and Math, New York University Abu Dhabi, Abu Dhabi, UAE

[2]Center for Systems Biology and Faculty of Industrial Engineering, Mechanical Engineering and Computer Science, School of Engineering and Natural Sciences, University of Iceland, Reykjavik, Iceland

[3]Center for Genomics and Systems Biology (CGSB), New York University Research Institute, New York University Abu Dhabi, Abu Dhabi, UAE

[4]Core Technology Platforms, New York University Abu Dhabi, Abu Dhabi, UAE

[5]Department of Biology, United Arab Emirates University (UAEU), Al Ain, UAE

[6]Lead Contact

*Correspondence: wf21@nyu.edu (W.F.), ksa3@nyu.edu (K.S.-A.)

https://doi.org/10.1016/j.isci.2020.101424

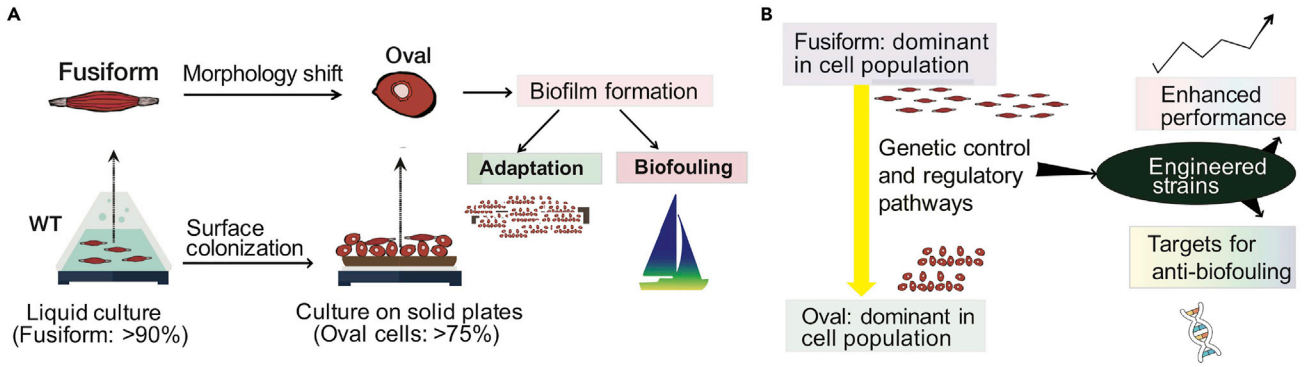

Figure 1. An Overview of the Morphotype Shifting of the Model Diatom *P. tricornutum* Associated with Surface Colonization

(A) Natural cell morphology shift in diatoms as an indicator for biofilm formation. There are multiple morphotypes in *P. tricornutum cultures*; of these, the fusiform cells are dominant in liquid growth under non-stress conditions and the oval cells dominate benthic growth and surface colonization. Fusiform cells gradually shift to oval cells during surface colonization or when subjected to other environmental stress, before biofilm formation and biofouling.

(B) By comparing gene expression profiles of different *P. tricornutum* morphotypes, putative regulatory pathways and gene products can be identified. The role of these candidate effectors can be validated by their expression in engineering strains. Once confirmed, the identified gene products can be used as targets in future studies to reverse the natural surface colonization process of diatoms in oceans to combat biofouling.

(De Martino et al., 2007, 2011), it has been reported that only the oval cell morphotype of *P. tricornutum* can adhere to surfaces and give rise to colonies to form compact biofilms (Stanley and Callow, 2007).

Diatoms have evolved intricate signaling pathways in response to environmental fluctuations, allowing them to be the dominant clade of microalgae in oceans (Thompson and Coates, 2017). Among the signaling pathways in cell differentiation and morphogenesis (Basson, 2012), G-protein-coupled receptor (GPCR) signaling pathway is highly conserved across eukaryotes and plays an essential role in signal transduction and response to extracellular stimuli (Chan et al., 2015; Cohen et al., 2017; Port et al., 2013). GPCRs, also known as seven-transmembrane domain receptors, are present in most organisms and mediate many vital signaling processes and physiological functions through their interactions with G proteins and downstream effectors (Shaw et al., 2019). Fungal GPCR-mediated signaling and the understanding of receptor-ligand interactions could facilitate the development of receptor-interfering compounds for disease control (Brown et al., 2018). By manipulating the expression levels of the GPCR components, researchers have engineered the yeast *Saccharomyces cerevisiae* and tuned the receptor and reporter to function in a controllable manner to obtain a platform for biosensor applications (Shaw et al., 2019).

Here, we interrogate the molecular mechanism underlying the morphological shift in *P. tricornutum* (strain Pt1 8.6_F) in relation to surface colonization (Figure 1). The Pt1 8.6_F strain of *P. tricornutum* was selected as the model in our study as this strain is known to be an optimal reference model for genetic and genomic studies (Fu et al., 2017), with the ability to shift its morphotypes during surface colonization and biofilm formation, in addition to the availability of its complete genome sequence (Bowler et al., 2008). We identify a set of signaling genes that are differentially regulated during morphotype switching. We demonstrate that engineering the strain to overexpress a *GPCR* gene is sufficient to shift the dominant morphotype from fusiform to oval cells during non-stress growth conditions. The engineered strain also achieves similar photosynthesis performance as its fusiform wild-type (WT) counterpart, and it shows more resistance to UV stress, indicating its potential biotechnological applications.

RESULTS

Genome-wide Transcriptome Analysis of Two Different Morphotype Cultures

To identify transcriptional shift of cells between solid culture (oval > 75%) and liquid culture (fusiform > 75%), we performed RNA sequencing (RNA-seq) on RNA isolated from the WT *P. tricornutum* strain Pt1 8.6_F grown in liquid and on solid media under low light intensity of 30–50 μmol photons m^{-2} s^{-1} (see Methods). The genome sequence of *P. tricornutum* (ASM15095v2 [2013-07-EBI-Phatr3]) was used as a reference to align the transcriptome reads, and normalized counts were calculated to characterize gene expression in cells (see Methods). Among all the expressed genes detected, differentially expressed genes (DEGs) were identified with a threshold of greater than 2-fold and a false discovery rate (FDR) of <0.05.

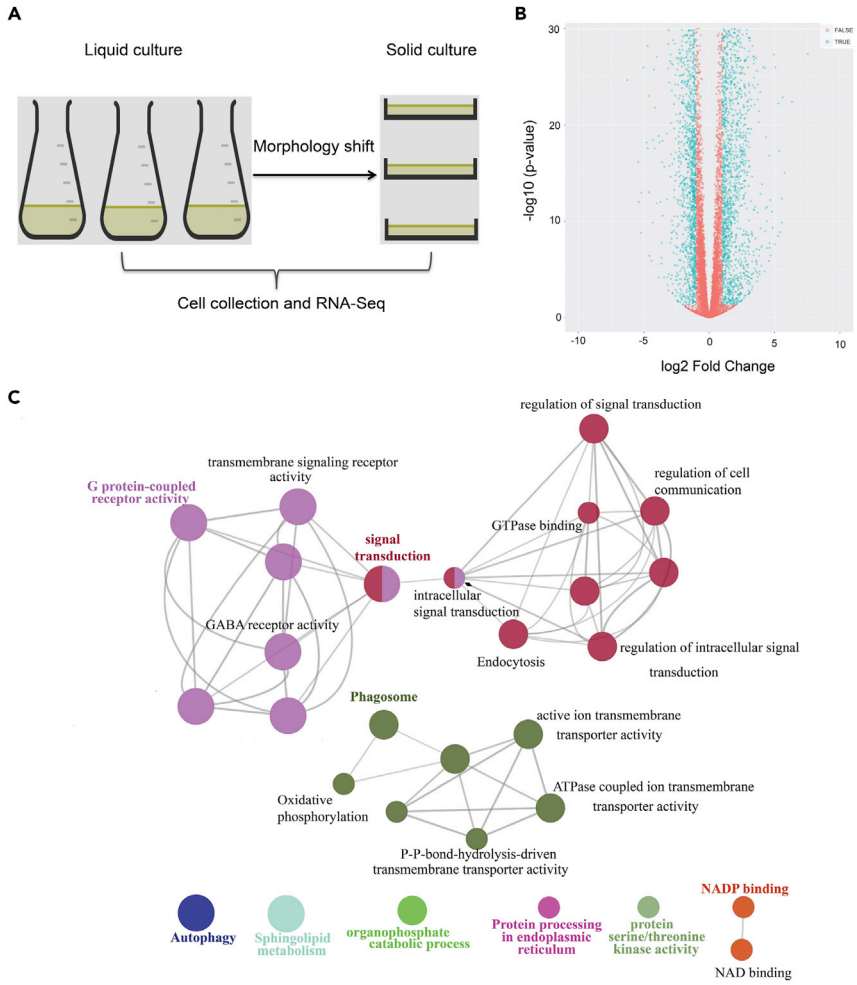

Figure 2. Global Transcriptomic Analysis and Identification of DEGs

Figure360▷ For a Figure360 author presentation of this figure, see https://doi.org/10.1016/j.isci.2020.101424.

(A) Liquid culture (fusiform cells in population >90%) and solid culture (oval cells in population >75%) of the model diatom *P. tricornutum* Pt1 8.6_F were generated and cells were collected for RNA-seq.

(B) Volcano plot with p values and fold changes as log-scaled axes. DEGs are identified with a threshold of $\log_2$(fold changes) > 1 and a significance level of FDR < 0.05. Significant differences at p value < 0.05 with >2-fold changes are shown in blue color.

(C) Gene set enrichment analysis of up-regulated signaling genes highlighting the GPCR signaling pathway. A group of 61 identified signaling genes was used for analysis. GO terms are represented as nodes in the graph, each pathway and its related nodes were presented with a unique color ($p < 0.05$), and node sizes indicate the relative numbers of genes that represent the GO term, whereas the edges represent genes shared between the GO terms.

A total of 2,468 genes were up-regulated and 1,878 genes were down-regulated in the solid WT (Figure 2 and Table S1) when compared with the liquid WT cells.

Gene set enrichment analysis (GSEA) (Bindea et al., 2009; Love et al., 2014) was carried out to identify overrepresented Gene Ontology (GO) terms for DEGs from the WT, highlighting cellular biosynthetic processes and signaling-related GO terms in up-regulated genes (Figure S1) and photosynthesis-related GO terms in down-regulated genes (Figure S2). We then performed KEGG Orthology annotations (Figure S3) on a total of 2,468 up-regulated genes from the WT using the KEGG Automatic Annotation Server (http://www.genome.jp/tools/kaas/) and identified 61 genes involved in 44 potential signaling pathways (Figure 2 and Table S2). GSEA for the 61 signaling genes revealed that the GPCR signaling pathway was significantly enriched and five known GPCR-encoding genes, i.e., *GPCR1A* (Phatr3_Jdraft1756), *GPCR1B* (Phatr3_J54411), *GPCR2* (Phatr3_Jdraft1740), *GPCR3* (Phatr3_J44131), and *GPCR4* (Phatr3_J44133), as well as three predicted GPCR genes

(Phatr3_J47068, Phatr3_J49346, and Phatr3_J35620) were up-regulated in the solid culture of *P. tricornutum* when compared with its liquid culture counterpart (Figure 2). A protein-protein interaction network was also predicted using these 61 signaling genes (59 of 61 were identified in the database) based on the STRING database (Figure S4). We note that the network is fragmented due to the lack of experimental evidence in diatoms.

GPCR1A Transformants Show Distinct Morphological Shift and Strong Resistance to Light Stress

We queried the KEGG Orthology annotation server with the 2,468 up-regulated genes and identified 61 signaling genes among them. To experimentally interrogate their potential roles in the morphological shift, we synthesized a group of 14 candidate signaling genes with a focus on several GPCR genes because GPCRs are on the top level of signal transduction hierarchy (Figure S5). We expressed these individually in *P. tricornutum* cells (Miyahara et al., 2013) with a controllable nitrate reductase promoter (see Methods) to test their ability to shift the cell morphology from fusiform to oval forms. We observed that cells transformed with either a *GPCR1A* or a *GPCR4* construct shifted the population to be dominated by the oval cells.

We conducted surface colonization experiments with these GPCR transformants (i.e., GPCR1A transformants and GPCR4 transformants) on glass slides and found that both transformants showed much stronger attachment and developed more clumps on glass slides over 72 h when compared with their WT counterpart (Figure S6). The oval cell morphotype-dominant transformants were able to colonize surfaces effectively and showed stronger adhesion patterns than their WT counterpart (Figure S6). These results are also in line with those of previous studies on the adhesion strength of different *P. tricornutum* species (De Martino et al., 2011; Stanley and Callow, 2007).

The GPCR1A transformants were selected for further experimental investigation. The typical cell morphotypes of the GPCR1A transformants and WT in liquid culture under non-stress growth conditions were observed by light and scanning electron microscopies (Figures 3A and 3B). The average cell size of the GPCR1A transformants (Table S3) in liquid culture was 6.63 $\pm$ 0.12 μm, which is similar to that of WT cells on solid culture (6.35 $\pm$ 0.12 μm) but significantly larger ($p = 0.0016$) than those of the cells in liquid culture (5.13 $\pm$ 0.25 μm). The transformed oval cells were morphologically similar to the WT oval cells.

To evaluate the strain capability in response to immediate light stress, we determined the effective quantum yields (QY) of photosystem II (PSII) of the transformants using the WT as controls under light stress of 220 μmol photons m^{-2} s^{-1} (Figure 3C). The effective QYs of the transformants were similar to those of the WT of liquid culture (Figure 3C). Moreover, the effects of UV treatment on different strains were studied (Figure 3D) to assess the role of diatom frustules in UV protection as silica cell walls in diatoms can protect DNA from UV light damage (Aguirre et al., 2018). As indicated by their different survival rates ($p = 0.031$), we found that the transformant cultures, with >75% oval cells, were more resistant to UV-C than the WT cultures of over 90% fusiform cells (Figure 3D). This result indicates that the oval cell form could provide an additional layer of protection against UV irradiation damage.

Comparative Transcriptomics and Reconstruction of Signaling Network during Surface Colonization

The GPCR1A transformants displayed oval cells as the dominant form in the population when compared with their WT counterparts under the same non-stress growth condition (Figure S6). The transcriptome analysis of GPCR1A transformants identified 1,568 up-regulated genes and 1739 down-regulated genes when compared with its WT counterpart in liquid culture (Table S4). The DEGs are fewer in the transformants than in the solid WT. Furthermore, 685 of the 1,568 up-regulated genes in the transformants were shared with the identified up-regulated DEGs in the solid WT during the surface colonization process (Figure 4). Among the 685 up-regulated DEGs, four GPCR genes including *GPCR1A*, *GPCR1B*, *GPCR3*, and *GPCR4* were highly expressed in the transformants when compared with their WT counterpart in the liquid culture, showing a similar signaling pattern as the solid WT growing on agar plates (Figure 4 and Table S4). However, the fold changes of the top 100 up-regulated genes from the solid WT, ranging from 21.0 to 279.8 with a median level of 36.2, were much higher than those from transformants, ranging from 8.3 to 143.7 with a median level of

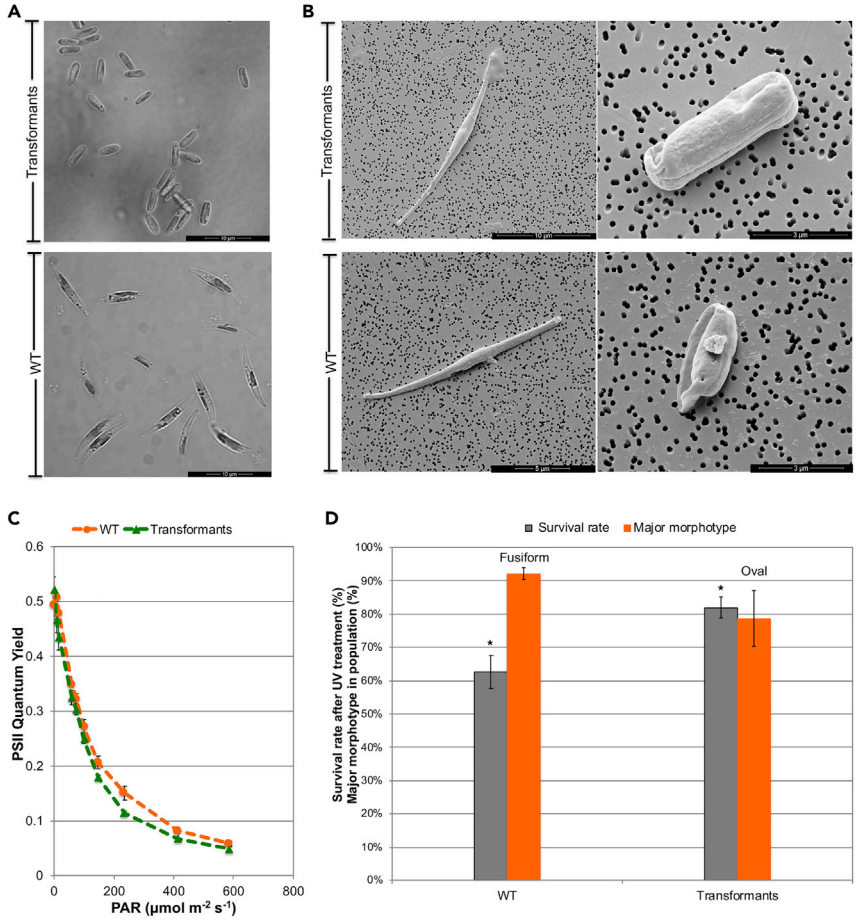

Figure 3. Morphological Shift in the Diatom Population and Its Characteristics

(A) Bright-field microscopic images showing the dominant morphotypes in the GPCR1A transformants when compared with the wild-type (WT).

(B) Scanning electron microscopic images of different morphotypes in transformants and WT.

(C) Determination of the theoretical photosynthetic efficiency (F_v/F_m) and effective quantum yield (QY) of photosystem II under a light intensity of 220 µmol photons m^{-2} s^{-1}.

(D) Enhanced cell resistance to UV radiation in transformants (with oval cells at >75% of the population) when compared with the wild type (with oval cells at <10% of the population). Values were averaged from either two or three independent experiments. WT, wild-type; PAR, photosynthetically active radiation. Error bars indicate SEM. * Indicates statistical significance between the groups ($p < 0.05$).

12.1 (Table S5). In addition, 14 of 16 shared genes of the two top-100 lists (Table S5) were at much greater fold changes in the solid WT, indicating that the expression shift was moderate in the transformants compared with those in the condition of harsh environmental stress (e.g., surface colonization). As a consequence of GPCR1A overexpression, downstream effector and regulator genes, including a GTPase-binding protein gene (Phatr3_J26387) and a protein kinase C gene (Phatr3_J14202), were also found to be up-regulated in the transformants. In addition to the GPCR signaling genes and their downstream effectors, we analyzed the transcription factors (TFs) from the two groups of DEGs, i.e., GPCR1A transformants and the solid WT, when compared with the liquid WT (Figure 5). Although many TF families showed both up- and down-expression pattern, one TF, PHF5-like protein (PHD finger-like domain-containing protein 5A), was up-regulated both in the solid culture and in the transformants, when compared with the liquid WT. We note that PHF5-like proteins are reported with a role in cell cycle progression in yeast and morphological development in worms (Oltra et al., 2004).

We reconstructed and manually curated the proposed GPCR-mediated signaling pathway based on the integration of up-regulated DEGs in solid culture when compared with liquid culture information using

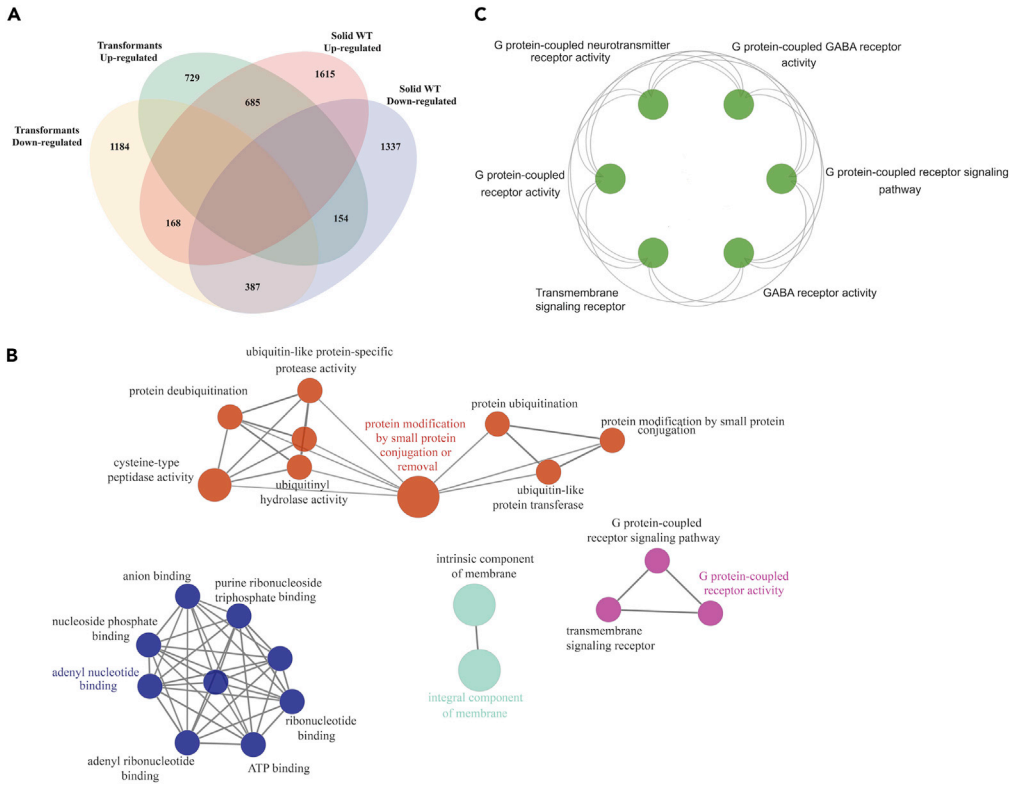

Figure 4. Comparative Analysis of Gene Expression Profiles upon Morphological Shift in Engineered and Wild-Type Strains

(A) Venn diagram of shared and unique genes between transformants-derived and solid culture condition-derived DEGs.
(B) Gene ontology analysis of the shared, up-regulated DEGs showing the significantly enriched ($p < 0.05$) terms shared between transformants-derived and solid culture condition-derived morphological shift from fusiform to oval cells.
(C) Gene ontology analysis of the signaling genes (a subset of up-regulated DEGs in the transformants) highlighting the significant enrichment of GPCR-related signaling pathways.

KAAS (KEGG Automatic Annotation Server, Tables S1, S2, and S6). The proposed pathways included major up-regulated signaling genes as a consequence of growth on solid media (Figure 6 and Table S6). Key effectors for the surface colonization process, including AMPK, cAMP, FOXO, MAPK, and mTOR signaling pathways and their related kinases and activators, are proposed (Figure 6). Among the 32 up-regulated signaling genes in the solid WT when compared with the liquid WT, only 11 signaling genes were found to be up-regulated in the transformants compared with their liquid WT counterpart (Figure 6). The transformants appeared capable of shifting the dominant morphotype from fusiform to oval cells with fewer up-regulated signaling genes than in the solid WT (Figure 6 and Table S6). Moreover, the fold changes of four of the GPCR signaling genes, i.e., *GPCR1A*, *GPCR1B*, *GPCR3*, and *GPCR4*, were 2.87 $\pm$ 0.07 (n = 3, $\pm$SEM), 2.41 $\pm$ 0.11, 2.55 $\pm$ 0.04, and 2.86 $\pm$ 0.08 times, respectively, when compared with their liquid WT counterparts; these fold differences were statistically significant (FDR < 0.05). However, the fold change of expression in these GPCR genes in transformants only ranged from 2.41 to 2.87. In contrast, the fold changes for these genes ranged from 4.14 to 49.18 in the solid WT when compared with the liquid WT (Tables S2 and S4), indicating that the expression changes of GPCR signaling genes were more affected by environmental factors.

A schematic wiring diagram of the key signaling components and the downstream targets is illustrated, and the polyamine pathway is highlighted (Figure S7). We note that polyamines play an important role in the promotion of silica precipitation for the formation of siliceous shells of diatoms (Kroger, 2007). Genes encoding well-known cell wall proteins such as silaffins have not been identified in *P. tricornutum*; however, the up-regulation of major genes involved in the polyamine pathway alludes to the role of polyamines in the construction of the frustule during oval cell formation (Figure S7).

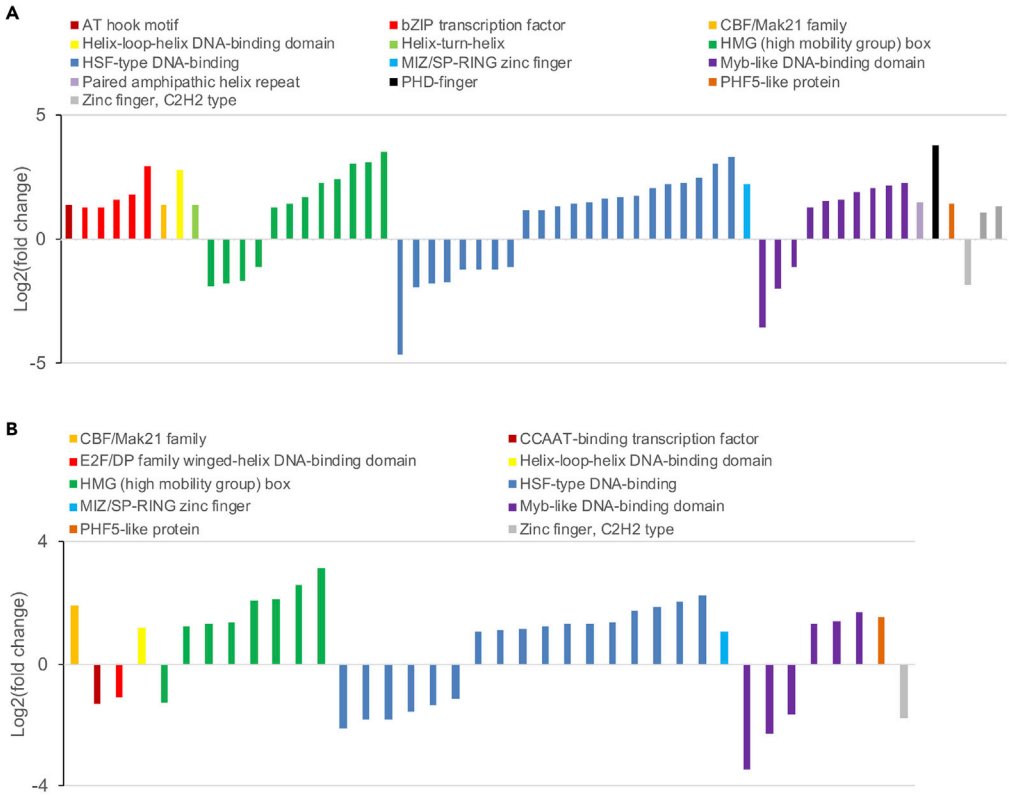

Figure 5. Differential Expression of Transcription Factors

(A and B) The expression of transcription factors (TFs) was compared between wild-type (WT) cells grown on solid medium and in liquid (A) and between GPCR1A transformants grown in liquid culture and WT cells grown in liquid (B). The bar graphs represent TF families and their genes with their expression level shown as $\log_2$ of their fold change. TF annotations for the model diatom *P. tricornutum* were obtained from https://phycocosm.jgi.doe.gov/mycocosm/annotations/browser/transfactor/summary;zEFxC9?p=Phatr2.

DISCUSSION

The model diatom *P. tricornutum*, a planktonic species that also has a benthic morphotype (i.e., oval cell form), usually appears as fusiform in liquid cultures under non-stress conditions, and it contributes to biofilm formation and biofouling upon morphology shift and surface colonization (Thompson and Coates, 2017). The cell and molecular biology of biofouling are largely unknown, even though environment-friendly antifouling coatings are urgently needed. In this study, we identified a group of 61 signaling genes involved in *P. tricornutum* during the morphological shift of cell populations (Figures 4 and S3). These up-regulated signaling genes include five annotated GPCR genes in diatoms, i.e., *GPCR1A*, *GPCR1B*, *GPCR2*, *GPCR3*, and *GPCR4*. We note that these GPCRs might also be involved in responding to sexual cues in diatoms, such as the planktonic species *Pseudo-nitzschia multistriata* (Basu et al., 2017). In this study, we transformed the WT model diatom species, *P. tricornutum*, with GPCR expression constructs, to shift its morphotype and demonstrated that the engineered strain enhanced its resistance to UV light. Moreover, we show that the induced expression of GPCR1A is sufficient to shift morphotypes, pointing to this protein as a potential target protein of screening anti-biofouling compounds. A comparative RNA-seq study on *Phaeodactylum* morphotypes was recently reported on the strain Pt3 (Ovide et al., 2018), in which the major morphotype is oval (60%–75%) under liquid culture conditions. This phenotypic ratio is uncommon and is different in other strains of *P. tricornutum*, in which the major morphotype is fusiform (De Martino et al., 2007).

In addition to the observed cell differentiation in diatoms, other eukaryotic microorganisms, such as the yeast, are able to differentiate into specific subpopulations with different characteristics to form organized microbial communities such as biofilms, colonies, and pseudohyphae on solid surfaces with unique

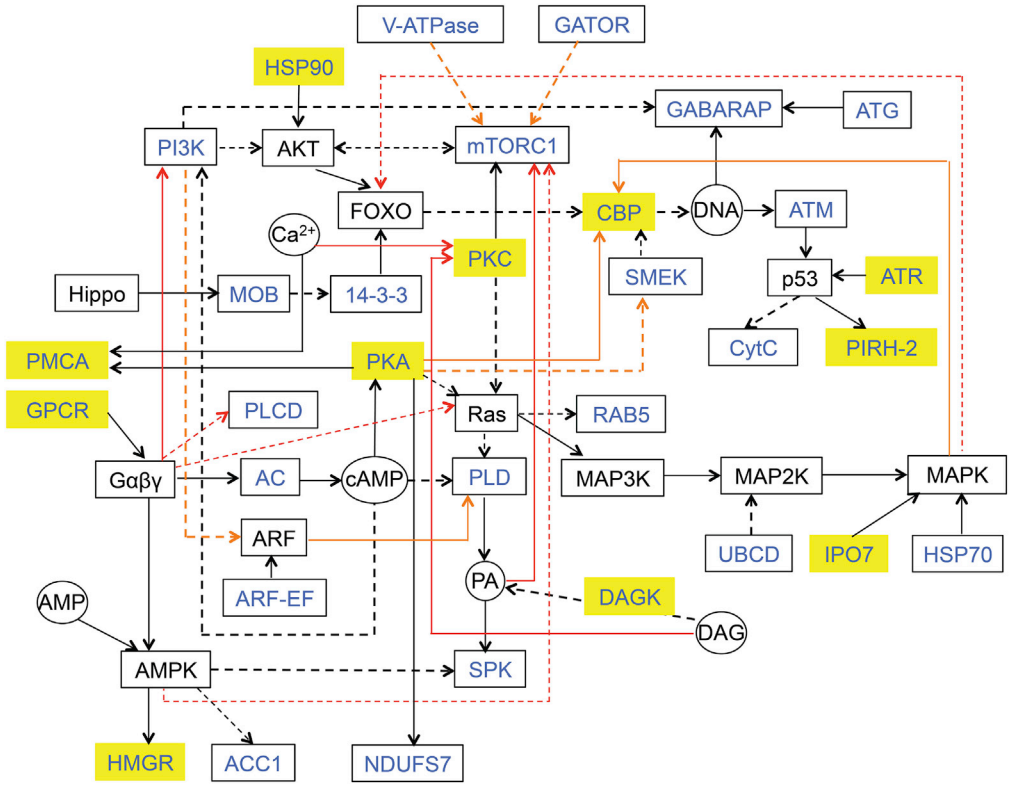

Figure 6. A Reconstructed Putative Signaling Network Involved in Surface Colonization

The *P. tricornutum* signaling network reconstruction was done using information obtained from KAAS (KEGG Automatic Annotation Server), as well as through manual curation. Annotations were obtained by performing BLAST and assigning orthologs by the BBH (bidirectional best hit) method, against the manually curated KEGG GENES database. Compounds are indicated within circles: AMP, 5′-adenosine monophosphate; Ca^{2+}, calcium cation; cAMP, cyclic AMP; DAG, diacylglycerol; PA, phosphatidic acid. Proteins are indicated in square-shaped boxes: 14-3-3, 14-3-3 protein epsilon; AC, adenylate cyclase 1; ACC1, acetyl-CoA carboxylase/biotin carboxylase 1; ARF-EF, ARF guanyl-nucleotide exchange factor; ATG, autophagy-related protein; ATM, serine-protein kinase ATM; ATR, serine/threonine-protein kinase ATR; CBP, E1A/CREB-binding protein; CytC, cytochrome *c*; DAGK, diacylglycerol kinase; GABARAP, GABA(A) receptor-associated protein; GATOR, GATOR complex protein; GPCR, G-protein-coupled receptor; HMGR, hydroxymethylglutaryl-CoA reductase; HSP70, heat shock 70-kDa protein; HSP90, heat shock 90-kDa protein; IPO7, importin-7; MOB, MOB kinase activator; mTORC1, serine/threonine-protein kinase mTOR; NDUFS7, NADH dehydrogenase (ubiquinone) Fe-S protein 7; PI3K, phosphatidylinositol 3-kinase; PIRH-2, RING finger and CHY zinc finger domain-containing protein; PKA, protein kinase A; PKC, protein kinase C; PLCD, phosphatidylinositol phospholipase C, delta; PLD, phospholipase D1/2; PMCA, P-type Ca^{2+} transporter type 2B; SMEK, protein phosphatase 4 regulatory subunit 3; SPK, sphingosine kinase; UBCD, ubiquitin-conjugating enzyme E2 D; V-ATPase, V-type H+ -transporting ATPase. Detailed information on differentially expressed genes is included in Table S6. Solid-line arrows represented direct transduction between two proteins/compounds, whereas dashed-line arrows indicated multiple steps of transduction between two proteins/compounds. The coloring of the lines was done to enhance the diagram. Blue-colored text indicated that the genes encoding the proteins were up-regulated in solid wild-type (WT) culture compared with liquid WT culture, yellow-colored boxes represented the genes encoding the proteins that were up-regulated in liquid transformants culture compared with liquid WT culture; the gene expression information is based on whole-transcriptome analysis carried out in this study.

properties (Cap et al., 2012). The budding yeast *Saccharomyces cerevisiae* can differentiate from unicellular to pseudohyphal filamentous form in response to stress under the regulation of cyclic AMP-protein kinase A (cAMP/PKA) and the filamentation mitogen-activated protein kinase (fMAPK), rat sarcoma/protein kinase A (RAS/PKA), sucrose nonfermentable (SNF), and target of rapamycin (TOR) signaling pathways (Kim and Rose, 2015). Notably, GPCRs such as Gα subunit Gpa2 of the RAS pathway were recognized during cell differentiation to the filamentous form (Cullen and Sprague, 2012; Pothoulakis and Ellis, 2018). Furthermore, *S. cerevisiae* was found capable of forming one colony with two major

subpopulations, i.e., U and L cells, occupying the upper and lower colony regions, respectively, and the optimized metabolic properties for U cell long-term existence were activated and controlled by the glutamine-induced TOR pathway amino acid sensor systems (e.g., SPS) together with other signaling pathways under lowered respiration (Cap et al., 2012). Mpk1 (the MAPK) and Bck1 (the MEKK) as well as the receptors that activate and regulate the pathway together with Rlm1 (a TF phosphorylated and activated by Mpk1), all played important roles during yeast cell differentiation into sporulation in colonies (Piccirillo et al., 2015). In this study, PKA and mTOR signaling pathways were also found up-regulated during diatom surface colonization (Figure 6; Tables S1, S4, and S6). Moreover, PKA was up-regulated in the *GPCR1A* transformants when compared with its WT counterpart (Figure 6). These findings highlighted the common function of these signaling components during cell differentiation across the distant phyla of diatoms and yeast.

P. tricornutum is the only known diatom species that can grow without silicate and has a significant distinction between its two main morphotypes, i.e., fusiform and oval cells, and only oval cells form silicified cell walls (Tesson et al., 2009). With the function of matrix peptides and proteins, silicic acid is converted into amorphous hydrated silicon dioxide with nanostructural properties in diatom cells (Pamirsky and Golokhvast, 2013). However, there is no clear information on the native silaffins in *P. tricornutum*, The engineered strain demonstrated enhanced tolerance to UV stress when compared with the WT counterpart, most likely due to the silicified cell walls as diatom SiO_2 frustules can protect DNA from UV light (Aguirre et al., 2018; Ellegaard et al., 2016). It has also been reported that genetically engineered diatom biosilica can be used for targeted drug delivery (Delalat et al., 2015). These findings may facilitate developing UV stress-resistant strains in industries as well as designing novel applications in biomedicine (Baio et al., 2014).

Marine biofouling has long constituted a major problem for the global maritime and aquaculture industries to alleviate as it has adverse effects and increases operating costs significantly (Callow and Callow, 2011; Salta et al., 2013). The International Maritime Organization banned many traditional biocide-based antifouling coatings, including the very effective and widely used tributyltin (TBT) coatings at the beginning of the twenty-first century due to their high toxicity toward all organisms in the ecosystem and negative impacts on non-target organisms. In this context, an alternative antifouling technology has been in great demand, and much effort has been focused on developing environment-friendly antifouling systems (Magin et al., 2010). Recently, researchers started to explore biomimetic designs for antifouling methods that can combat fouling without toxic side effects (Bixler and Bhushan, 2012; Kang et al., 2016). Understanding the biology of biofouling is important for the development of a successful and robust nontoxic biofouling remedy. As diatoms are the dominant algal group in the ocean and also one of the early colonizers involved particularly in the micro-fouling stage in which biofilm is formed (Dang and Lovell, 2016; Salta et al., 2013), biological understanding of the molecular regulation underlying diatom biofilm formation and dispersal may be beneficial to develop new strategies to control and mitigate biofouling. *P. tricornutum* is a polymorphic pennate diatom capable of strong adhesion to the substrates, common in pennate diatoms that all mediate biofouling (Dugdale et al., 2006; Herbstova et al., 2017; Stanley and Callow, 2007). Our findings may pave the way for developing effective and environment-friendly antifouling technology with promising biological targets from signaling pathways. As such, the *GPCR1A* gene identified here is a promising antifouling target. Furthermore, its orthologs in other biofouling organisms can be considered targets to interrogate for developments of a universal, bio-based, antifouling strategy. As morphological shift is a coordinated process during cell development, other regulatory factors such as TFs (Figure 5) may also play important roles and could be of interest for future studies. We expect the novel findings and resources described in this study to serve as a starting point for the discovery of new antifouling targets in the future.

Limitations of the Study

P. tricornutum strain Pt1 8.6_F was used as an optimal model diatom species in this study as this strain can make a clear shift of morphotype from fusiform to oval cells during surface colonization. We identified and reconstructed a signaling network underlying surface colonization, highlighting the roles of signaling genes, including genes encoding GPCRs. However, the network analysis in this study relied on the reference genome sequence of *P. tricornutum* (2013-07-EBI-Phatr3), which is incomplete in functional annotations, as observable in KEGG pathway maps. As a consequence, there might be other key signaling genes and regulatory TFs involved that our study could not identify. In addition, although the analysis of the gene expression of the whole population allowed the identification of DEGs in conjunction with morphological shifts, our RNA-seq analysis looked at asynchronous populations of cells enriched in one or the other morphotype; therefore

our reported gene expression changes are limited to measurements of population averages and may not fully reflect the fold changes between individual morphotypes. Surface colonization is a long process (i.e., weeks), and the shift of dominant morphotype in population is a distinctive feature of *P. tricornutum* during such process and biofilm formation. There might be transient gene expression events that we likely could not cover with our approach as we only looked at gene expression changes at a single time point; however, our main goal was to identify gene products that could shift cell morphology and maintain it, which we were able to achieve. Finally, the identification of involved signaling genes was based on mRNA expression profiles and not protein levels due to the lack of antibodies for the detection of GPCRs in diatoms. Although we validated the role of *GPCR1A* experimentally, our analysis could have missed other effectors that their activity was modulated, but their expression level at mRNA level was not significantly altered.

Resource Availability

Lead Contact

Further information and requests for resources and reagents should be directed to and will be fulfilled by the Lead Contact, Kourosh Salehi-Ashtiani (ksa3@nyu.edu).

Materials Availability

All sequences of synthesized genes can be found in Table S7.

Data and Code Availability

RNA-seq data from this article can be found in the GenBank/NCBI data libraries (GenBank: PRJNA566271). The RNA-seq data have also been deposited in Dryad with a unique identifier (https://doi.org/10.5061/dryad.ns1rn8ppx).

METHODS

All methods can be found in the accompanying Transparent Methods supplemental file.

SUPPLEMENTAL INFORMATION

Supplemental Information can be found online at https://doi.org/10.1016/j.isci.2020.101424.

ACKNOWLEDGMENTS

Funding: Financial support for this work was provided by New York University Abu Dhabi Faculty Research Funds (AD060) and NYUAD Institute grant (73 71210 CGSB9). W.F. was additionally supported by the Icelandic Technology Development Fund (163922-0611). The authors thank Kenan S. Jijakli and Joseph Koussa for editing and comments on the generation of several figures. We thank the NYU Abu Dhabi Core Technology Platforms (CTP) and NYUAD Bioinformatics Core for assistance. We thank Marc Arnoux and Nizar Drou for help with high throughput sequencing and analysis.

AUTHOR CONTRIBUTIONS

W.F. and K.S.-A. designed the research and wrote the paper. W.F. performed the laboratory experiments, including vector construction, transformation, and strain validation, and analyzed the data. W.F., A.C., B.D., and A.J. performed transcriptome analysis. M.S. performed confocal microscopy experiments. W.F. and K.B. conducted morphotype analyses. W.F. and J.W. conducted scanning electron microscopic analyses. W.F. and M.S. performed the RNA-seq experiments. W.F., D.A.-K., S.D., A.M., and A.A. contributed to strain screening and PCR verification. J.W. carried out scanning electron microscopic imaging of diatom samples. All authors contributed to the editing of the manuscript.

DECLARATION OF INTERESTS

The authors declare no competing financial interests.

Received: January 8, 2020
Revised: April 25, 2020
Accepted: July 28, 2020
Published: August 21, 2020

REFERENCES

Aguirre, L.E., Ouyang, L.Q., Elfwing, A., Hedblom, M., Wulff, A., and Inganas, O. (2018). Diatom frustules protect DNA from ultraviolet light. Sci. Rep. *8*, 5138.

Baio, J.E., Zane, A., Jaeger, V., Roehrich, A.M., Lutz, H., Pfaendtner, J., Drobny, G.P., and Weidner, T. (2014). Diatom mimics: directing the formation of biosilica nanoparticles by controlled folding of lysine-leucine peptides. J. Am. Chem. Soc. *136*, 15134–15137.

Basson, M.A. (2012). Signaling in cell differentiation and morphogenesis. Cold Spring Harb. Perspect. Biol. *4*, a008151.

Basu, S., Patil, S., Mapleson, D., Russo, M.T., Vitale, L., Fevola, C., Maumus, F., Casotti, R., Mock, T., Caccamo, M., et al. (2017). Finding a partner in the ocean: molecular and evolutionary bases of the response to sexual cues in a planktonic diatom. New Phytol. *215*, 140–156.

Benoiston, A.S., Ibarbalz, F.M., Bittner, L., Guidi, L., Jahn, O., Dutkiewicz, S., and Bowler, C. (2017). The evolution of diatoms and their biogeochemical functions. Philos. T R. Soc. B *372*, 20160397.

Bindea, G., Mlecnik, B., Hackl, H., Charoentong, P., Tosolini, M., Kirilovsky, A., Fridman, W.H., Pages, F., Trajanoski, Z., and Galon, J. (2009). ClueGO: a Cytoscape plug-in to decipher functionally grouped gene ontology and pathway annotation networks. Bioinformatics *25*, 1091–1093.

Bixler, G.D., and Bhushan, B. (2012). Biofouling: lessons from nature. Philos. T R. Soc. A *370*, 2381–2417.

Bowler, C., Allen, A.E., Badger, J.H., Grimwood, J., Jabbari, K., Kuo, A., Maheswari, U., Martens, C., Maumus, F., Otillar, R.P., et al. (2008). The Phaeodactylum genome reveals the evolutionary history of diatom genomes. Nature *456*, 239–244.

Brown, N.A., Schrevens, S., van Dijck, P., and Goldman, G.H. (2018). Fungal G-protein-coupled receptors: mediators of pathogenesis and targets for disease control. Nat. Microbiol. *3*, 402–414.

Bruckner, C.G., Rehm, C., Grossart, H.P., and Kroth, P.G. (2011). Growth and release of extracellular organic compounds by benthic diatoms depend on interactions with bacteria. Environ. Microbiol. *13*, 1052–1063.

Callow, J.A., and Callow, M.E. (2011). Trends in the development of environmentally friendly fouling-resistant marine coatings. Nat. Commun. *2*, 244.

Cap, M., Stepanek, L., Harant, K., Vachova, L., and Palkova, Z. (2012). Cell differentiation within a yeast colony: metabolic and regulatory parallels with a tumor-affected organism. Mol. Cell *46*, 436–448.

Chan, W.K.B., Zhang, H.J., Yang, J.Y., Brender, J.R., Hur, J., Ozgur, A., and Zhang, Y. (2015). GLASS: a comprehensive database for experimentally validated GPCR-ligand associations. Bioinformatics *31*, 3035–3042.

Cohen, L.J., Esterhazy, D., Kim, S.H., Lemetre, C., Aguilar, R.R., Gordon, E.A., Pickard, A.J., Cross, J.R., Emiliano, A.B., Han, S.M., et al. (2017). Commensal bacteria make GPCR ligands that mimic human signalling molecules. Nature *549*, 48.

Cullen, P.J., and Sprague, G.F. (2012). The regulation of filamentous growth in yeast. Genetics *190*, 23–49.

Dang, H.Y., and Lovell, C.R. (2016). Microbial surface colonization and biofilm development in marine environments. Microbiol. Mol. Biol. R. *80*, 91–138.

De Martino, A., Bartual, A., Willis, A., Meichenin, A., Villazan, B., Maheswari, U., and Bowler, C. (2011). Physiological and molecular evidence that environmental changes elicit morphological interconversion in the model diatom Phaeodactylum tricornutum. Protist *162*, 462–481.

De Martino, A., Meichenin, A., Shi, J., Pan, K.H., and Bowler, C. (2007). Genetic and phenotypic characterization of Phaeodactylum tricornutum (Bacillariophyceae) accessions. J. Phycol. *43*, 992–1009.

De Tommasi, E., Gielis, J., and Rogato, A. (2017). Diatom frustule morphogenesis and function: a multidisciplinary survey. Mar. Genome *35*, 1–18.

Delalat, B., Sheppard, V.C., Ghaemi, S.R., Rao, S., Prestidge, C.A., McPhee, G., Rogers, M.L., Donoghue, J.F., Pillay, V., Johns, T.G., et al. (2015). Targeted drug delivery using genetically engineered diatom biosilica. Nat. Commun. *6*, 8791.

Dugdale, T.M., Willis, A., and Wetherbee, R. (2006). Adhesive modular proteins occur in the extracellular mucilage of the motile, pennate diatom Phaeodactylum tricornutum. Biophys. J. *90*, L58–L60.

Ellegaard, M., Lenau, T., Lundholm, N., Maibohm, C., Friis, S.M.M., Rottwitt, K., and Su, Y.Y. (2016). The fascinating diatom frustule-can it play a role for attenuation of UV radiation? J. Appl. Phycol. *28*, 3295–3306.

Finlay, J.A., Schultz, M.P., Cone, G., Callow, M.E., and Callow, J.A. (2013). A novel biofilm channel for evaluating the adhesion of diatoms to non-biocidal coatings. Biofouling *29*, 401–411.

Francius, G., Tesson, B., Dague, E., Martin-Jezequel, V., and Dufrene, Y.F. (2008). Nanostructure and nanomechanics of live Phaeodactylum tricornutum morphotypes. Environ. Microbiol. *10*, 1344–1356.

Fu, W.Q., Chaiboonchoe, A., Khraiwesh, B., Sultana, M., Jaiswal, A., Jijakli, K., Nelson, D.R., Al-Hrout, A., Baig, B., Amin, A., et al. (2017). Intracellular spectral recompositioning of light enhances algal photosynthetic efficiency. Sci. Adv. *3*, e1603096.

Garacci, M., Barret, M., Folgoas, C., Flahaut, E., Chimowa, G., Bertucci, A., Gonzalez, P., Silvestre, J., Gauthier, L., Zouine, M., et al. (2019). Transcriptomic response of the benthic freshwater diatom Nitzschia palea exposed to Few Layer Graphene. Environ. Sci. Nano *6*, 1363–1381.

Herbstova, M., Bina, D., Kana, R., Vacha, F., and Litvin, R. (2017). Red-light phenotype in a marine diatom involves a specialized oligomeric red-shifted antenna and altered cell morphology. Sci. Rep. *7*, 11976.

Kang, T., Banquy, X., Heo, J.H., Lim, C.N., Lynd, N.A., Lundberg, P., Oh, D.X., Lee, H.K., Hong, Y.K., Hwang, D.S., et al. (2016). Mussel-inspired anchoring of polymer loops that provide superior surface lubrication and antifouling properties. ACS Nano *10*, 930–937.

Kim, J., and Rose, M.D. (2015). Stable pseudohyphal growth in budding yeast induced by synergism between septin defects and altered MAP-kinase signaling. PLoS Genet. *11*, e1005684.

Kroger, N. (2007). Prescribing diatom morphology: toward genetic engineering of biological nanomaterials. Curr. Opin. Chem. Biol. *11*, 662–669.

Leterme, S.C., Le Lan, C., Hemraj, D.A., and Ellis, A.V. (2016). The impact of diatoms on the biofouling of seawater reverse osmosis membranes in a model cross-flow system. Desalination *392*, 8–13.

Levitan, O., Dinamarca, J., Hochman, G., and Falkowski, P.G. (2014). Diatoms: a fossil fuel of the future. Trends Biotechnol. *32*, 117–124.

Lewin, J.C., Lewin, R.A., and Philpott, D.E. (1958). Observations on phaeodactylum-tricornutum. J. Gen. Microbiol. *18*, 418.

Love, M.I., Huber, W., and Anders, S. (2014). Moderated estimation of fold change and dispersion for RNA-seq data with DESeq2. Genome Biol. *15*, 550.

Magin, C.M., Cooper, S.P., and Brennan, A.B. (2010). Non-toxic antifouling strategies. Mater. Today *13*, 36–44.

Miyahara, M., Aoi, M., Inoue-Kashino, N., Kashino, Y., and Ifuku, K. (2013). Highly efficient transformation of the diatom Phaeodactylum tricornutum by multi-pulse electroporation. Biosci. Biotechnol. Biochem. *77*, 874–876.

Mock, T., Otillar, R.P., Strauss, J., McMullan, M., Paajanen, P., Schmutz, J., Salamov, A., Sanges, R., Toseland, A., Ward, B.J., et al. (2017). Evolutionary genomics of the cold-adapted diatom Fragilariopsis cylindrus. Nature *541*, 536–540.

Oltra, E., Verde, F., Werner, R., and D'Urso, G. (2004). A novel RING-finger-like protein Ini1 is essential for cell cycle progression in fission yeast. J. Cell Sci. *117*, 967–974.

Ovide, C., Kiefer-Meyer, M.C., Berard, C., Vergne, N., Lecroq, T., Plasson, C., Burel, C., Bernard, S., Driouich, A., Lerouge, P., et al. (2018). Comparative in depth RNA sequencing of P. tricornutum's morphotypes reveals specific features of the oval morphotype. Sci. Rep. *8*, 14340.

Pamirsky, I.E., and Golokhvast, K.S. (2013). Silaffins of diatoms: from applied biotechnology to biomedicine. Mar. Drugs *11*, 3155–3167.

Piccirillo, S., Morales, R., White, M.G., Smith, K., Kapros, T., and Honigberg, S.M. (2015). Cell differentiation and spatial organization in yeast colonies: role of cell-wall integrity pathway. Genetics *201*, 1427–1438.

Port, J.A., Parker, M.S., Kodner, R.B., Wallace, J.C., Armbrust, E.V., and Faustman, E.M. (2013). Identification of G protein-coupled receptor signaling pathway proteins in marine diatoms using comparative genomics. BMC Genomics *14*, 503.

Pothoulakis, G., and Ellis, T. (2018). Synthetic gene regulation for independent external induction of the Saccharomyces cerevisiae pseudohyphal growth phenotype. Commun. Biol. *1*, 7.

Salta, M., Wharton, J.A., Blache, Y., Stokes, K.R., and Briand, J.F. (2013). Marine biofilms on artificial surfaces: structure and dynamics. Environ. Microbiol. *15*, 2879–2893.

Schaum, C.E. (2019). Enhanced biofilm formation aids adaptation to extreme warming and environmental instability in the diatom Thalassiosira pseudonana and its associated bacteria. Limnol. Oceanogr. *64*, 441–460.

Shaw, W.M., Yamauchi, H., Mead, J., Gowers, G.F., Bell, D.J., Oling, D., Larsson, N., Wigglesworth, M., Ladds, G., and Ellis, T. (2019). Engineering a model cell for rational tuning of GPCR signaling. Cell *177*, 782–796.e27.

Stanley, M.S., and Callow, J.A. (2007). Whole cell adhesion strength of morphotypes and isolates of Phaeodactylum tricornutum (Bacillariophyceae). Eur. J. Phycol. *42*, 191–197.

Tesson, B., Gaillard, C., and Martin-Jezequel, V. (2009). Insights into the polymorphism of the diatom Phaeodactylum tricornutum Bohlin. Bot. Mar. *52*, 104–116.

Thompson, S.E.M., and Coates, J.C. (2017). Surface sensing and stress-signalling in Ulva and fouling diatoms - potential targets for antifouling: a review. Biofouling *33*, 410–432.

Vanelslander, B., Paul, C., Grueneberg, J., Prince, E.K., Gillard, J., Sabbe, K., Pohnert, G., and Vyverman, W. (2012). Daily bursts of biogenic cyanogen bromide (BrCN) control biofilm formation around a marine benthic diatom. Proc. Natl. Acad. Sci. U S A *109*, 2412–2417.

Vardi, A., Thamatrakoln, K., Bidle, K.D., and Falkowski, P.G. (2008). Diatom genomes come of age. Genome Biol. *9*, 245.

iScience, Volume *23*

Supplemental Information

GPCR Genes as Activators of Surface Colonization Pathways in a Model Marine Diatom

Weiqi Fu, Amphun Chaiboonchoe, Bushra Dohai, Mehar Sultana, Kristos Baffour, Amnah Alzahmi, James Weston, Dina Al Khairy, Sarah Daakour, Ashish Jaiswal, David R. Nelson, Alexandra Mystikou, Sigurdur Brynjolfsson, and Kourosh Salehi-Ashtiani

Supplemental Information

Supplemental Information includes **Transparent Methods**, **eight figures**, and **seven tables** (shown as datasets in Excel files).

Transparent Methods

Algal culture and growth conditions

The strain, *P. tricornutum* Pt1 8.6_F (CCAP 1055/1, Culture Collection of Algae and Protozoa, Scottish Marine Institute, Scotland, UK), was used as a model diatom in this study. The wild type *P. tricornutum* was grown using f/2 +Si medium on either solid agar plates (for surface colonization) or in liquid culture (in flasks) under continuous cool white fluorescent lights of 50 μmol photons m^{-2} s^{-1} at 22° ± 2°C (Fu et al., 2017). Cell quantification was performed by determining the absorbance (at 600 nm) using a spectrophotometer regularly.

Chlorophyll fluorescence measurements for photosynthetic parameters

Chlorophyll fluorescence was measured using a PHYTO-PAM-II (Heinz Walz GmbH). The maximum photosynthetic efficiency of PSII was determined as $F_v/F_m = (F_m - F_o)/F_m$, where F_m is the maximal fluorescence, and F_o is the ground fluorescence in the dark- or low-light adapted cells. The effective quantum yield of PSII in cells was determined as F_v'/F_m' when exposed to the white light of 220 μmol photons m^{-2} s^{-1} over 10 minutes, where F_m' is the maximum fluorescence emission level in the light-acclimated cells. The relative electron transport rate (Cohen et al.) was also obtained for samples during the same experiments.

Generation of genetically modified *P. tricornutum* cells

A group of 14 cDNAs encoding candidate signaling genes (Gene IDs: Phatr3_J22677, Phatr3_J41807, Phatr3_Jdraft1756, Phatr3_J10677, Phatr3_J54411, Phatr3_EG02512, Phatr3_J51511, Phatr3_J12877, Phatr3_J2097, Phatr3_Jdraft1000, Phatr3_J54505, Phatr3_J55230, Phatr3_Jdraft1740, and Phatr3_J44133), including GPCR genes (as shown in Table S7), were synthesized and cloned in the shuttle vector pPha-NR (Fu et

al., 2017) with a nitrate reductase promoter by Twist Bioscience (San Francisco, CA, U.S.A.). The plasmids were then extracted from the bacterial cell cultures using the Qiagen Plasmid Mini kit (Hilden, Germany) after growth and selection in the presence of ampicillin (100 µg/ml). For the transformation of signaling genes in the diatom *P. tricornutum* (Miyahara et al., 2013), the multipulse electroporation protocol was followed as previously described (Fu et al., 2017). PCR verification of the transformants was conducted using genomic DNA and specific primers (**Fig. S8**).

Sample preparation, RNA extraction, and transcriptome sequencing (RNA-seq)

For solid culture experiments of wild type *P. tricornutum*, cells were grown on solid agar (1.2% agar plus the growth medium) for approximately two weeks, while control liquid cultures were grown in flasks for approximately one week (OD_{600}=~0.3). Both culture types were generated using f/2 +Si medium under continuous cool white fluorescent lights of 50 µmol photons m^{-2} s^{-1} at 22° ± 2°C. Cells were collected during the exponential phase for RNA extraction. For each group, three independent experiments were conducted, and triplicates of samples were collected for RNA sequencing studies.

For comparison between the transformed (engineered) *P. tricornutum* and its wild type counterpart, both cultures were grown under the same conditions, in liquid, using f/2 +Si medium in flasks for approximately one week under continuous cool white fluorescent lights of 50 µmol photons m^{-2} s^{-1} at 22° ± 2°C. Cultures were added with 5.0 mM KNO_3 for one day, and cells were collected during the exponential phase for RNA extraction. For each group, three independent experiments were carried out, and triplicate samples were collected for RNA extraction.

Total RNA extraction was performed using the MagMAX-96 Total RNA Isolation kit AM1830 with all necessary reagents (Thermo Fisher Scientific Inc.) according to the manufacturer's instruction. The complementary DNA (cDNA) libraries were prepared using the TruSeq RNA Library Preparation kit v2 (Illumina) according to the manufacturer's instruction, as previously described (Fu et al., 2017). After quality inspection, the library was quantified by quantitative PCR for cluster generation on the Bot system and then

sequenced using paired-end sequencing of 2 × 100–base pair read length on an Illumina HiSeq 2500 system (Illumina).

Quantitative comparison of gene expression, and gene set enrichment analysis (GSEA)

The genome sequence of *P. tricornutum* (2013-07-EBI-Phatr3) was used as a reference to align the transcriptome reads (http://protists.ensembl.org/Phaeodactylum_tricornutum/Info/Annotation/). To characterize gene expression in different samples, DESeq2 (Love et al., 2014) was used to identify DEGs between two groups of samples (triplicates within each group). Following the removal of the raw read count <10 in each sample, the total read count was normalized using DESeq2, which scales the read counts by a reference sample based on the geometric mean of the read counts across all samples. RPKM (Reads Per Kilobase of transcript, per Million mapped reads) was used as a normalized unit of transcript expression. Functional analysis and GSEA of DEGs were performed using ClueGO plugin (v2.5.0) in Cytoscape (v3.6.0; (Bindea et al., 2009). ClueGO determined the statistical overrepresentation of GO terms associated with the identified DEGs. The P values were calculated using a two-sided hypergeometric test, and Benjamini-Hochberg false discovery rate (FDR) correction was used to identify the statistical significance of GO terms with corrected $P < 0.05$ for multiple testing. The network was automatically laid out based on the ClueGO visual style, where nodes represented the GO terms, the node size referred to the number of genes in a particular GO, and the color of the nodes reflected the enrichment significance of the GO terms.

Surface colonization on glass slides

Glass microscope slides were first rinsed with deionized water then soaked in 1M HCl for 24 h (Stanley and Callow, 2007). The acid was removed by rinsing the slides using deionized water. The slides were rinsed and dried before adding the prepared diatom culture. The wild type, GPCR1A transformants, and GPCR4 transformants were cultivated under the same condition, then collected during exponential growth. Cells numbers were determined using a hemocytometer under a microscope for all strains. The same amount of cells

(500,000 cells/ml) were used in each experiment. Slides were placed in individual compartments of culture dishes, and 15 ml of cultures at the correct dilution were added. Three replicates were used for each experiment. The cells were allowed to settle for 72 h at 22±2°C in growth chambers, after which the slides were gently shaken/rinsed to remove unattached cells on a shaker at 150 rpm. Cells were then counted from each of the three replicate slides after recording microscope images from 9 randomly sampled views to provide cell adhesion and colonization data.

Statistical analysis

A student's t-test was performed to evaluate the significance of the difference between the two groups of samples for physiology data (p-value < 0.05).

Supplementary figures and figure legends

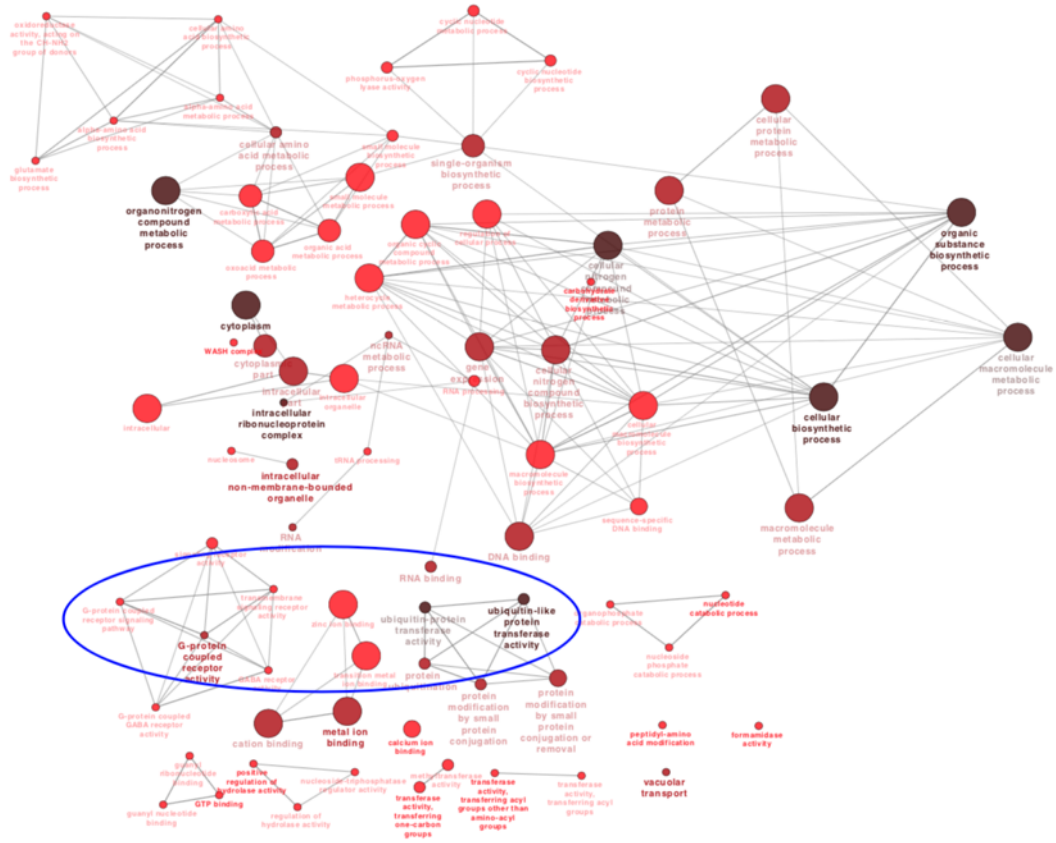

Fig. S1. Gene set enrichment analysis (GSEA) of up-regulated DEGs, related to Figure 2. GSEA was carried out to identify the overrepresented gene ontology (GO) terms for biological process, and molecular function of 2468 identified differentially expressed genes (DEGs) between wild type (WT) strain grown on solid media compared to liquid media growth. Node sizes indicate the relative numbers of genes that represent a GO term; GO terms are represented as nodes in the graph, the color gradient (red to dark red) represents the statistical term enrichment significance ($P < 0.05$). The blue circle marks the GO terms related to signaling pathways.

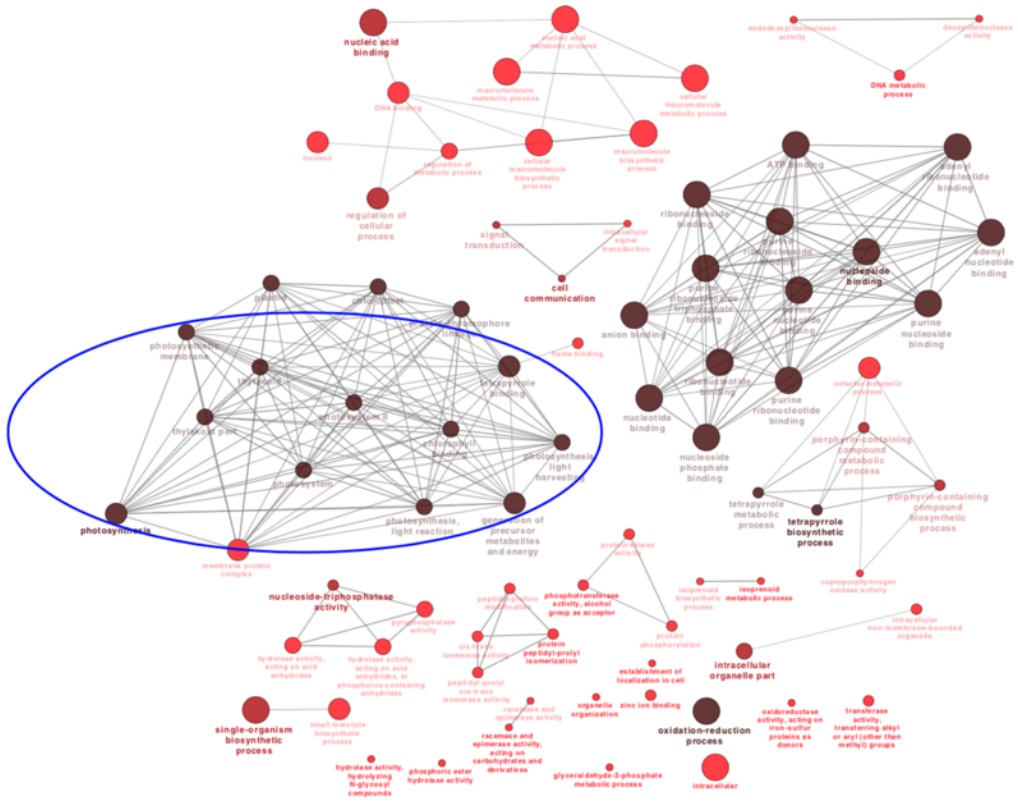

Fig. S2. GSEA of down-regulated DEGs, related to Figure 2. The 1878 DEGs were used to identify overrepresented gene ontology (GO) terms for biological process and molecular function between the growth of WT on solid media in comparison with liquid growth. Node sizes indicate the relative numbers of genes representing a GO term; GO terms are represented as nodes in the graph, the color gradient (red to dark red) represents the statistical term enrichment significance ($P < 0.05$). Blue circle highlights the GO terms identified in relation to photosynthetic processes.

Fig. S3. Identification of signaling pathways and genes using BLAST functional annotation and pathway mapping, related to Figure 2. The sequences of the 2468 up-regulated genes in the WT were searched by BLAST against the manually curated KEGG GENES database (https://www.genome.jp/kegg/kaas/) with a complete genome of *P. tricornutum* using BBH (bi-directional best hit of nucleotide by its default setup) to assign orthologs and provide functional annotation and pathway mapping through KEGG Automatic Annotation Server. The signaling pathways are marked with red boxes. Detailed gene IDs of the 61 identified signaling genes are described in Supplementary Table 2.

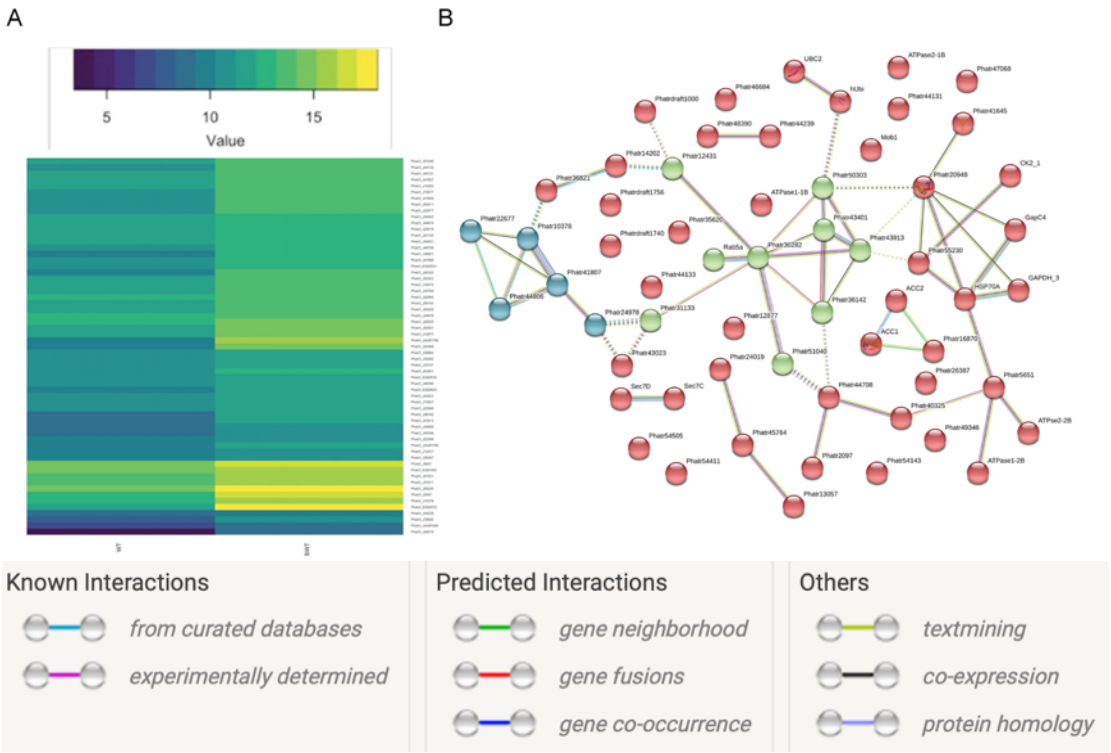

Fig. S4. Gene expression profile of 61 identified signaling genes, related to Figure 3. **(A)** A heatmap of the identified up-regulated signaling genes in the wild type. The color key represents the value of $\log_2$ (Normalized counts) of RPKM values. **(B)** Reconstruction of gene association network using the up-regulated signaling genes using the STRING database (https://string-db.org). The network is grouped using k-means clustering (with k=3). Nodes represent genes, and node colors represent the k-mean clustering; edge (link) colors indicate the type of evidence for the interactions. Known interactions, predicted interactions, and other interactions are indicated in the lower panel of the figure.

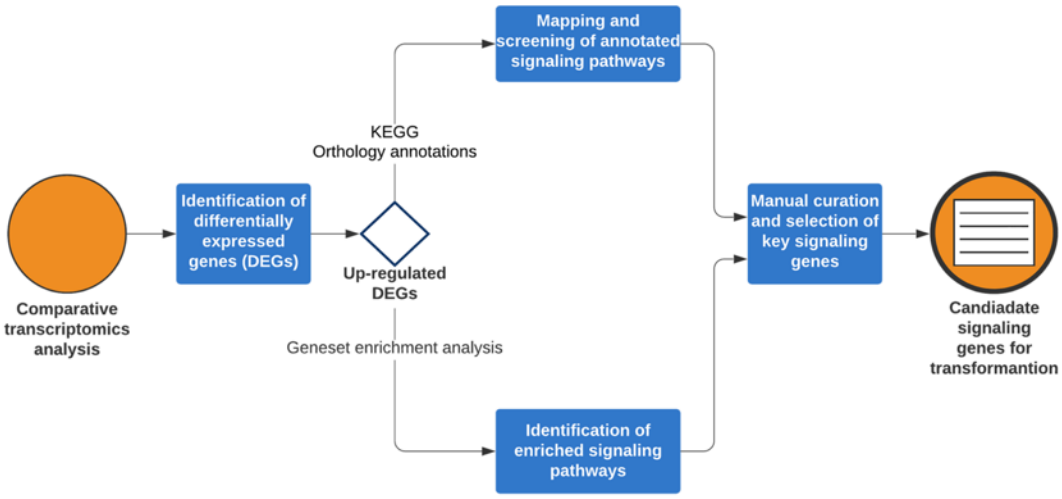

Figure S5. A workflow for screening and selection of candidate genes for overexpression in *P. tricornutum*, related to Figure 3. The principal selection criteria are based on the integration of gene expression information with computational enrichment analyses and manual curation of the results, as shown.

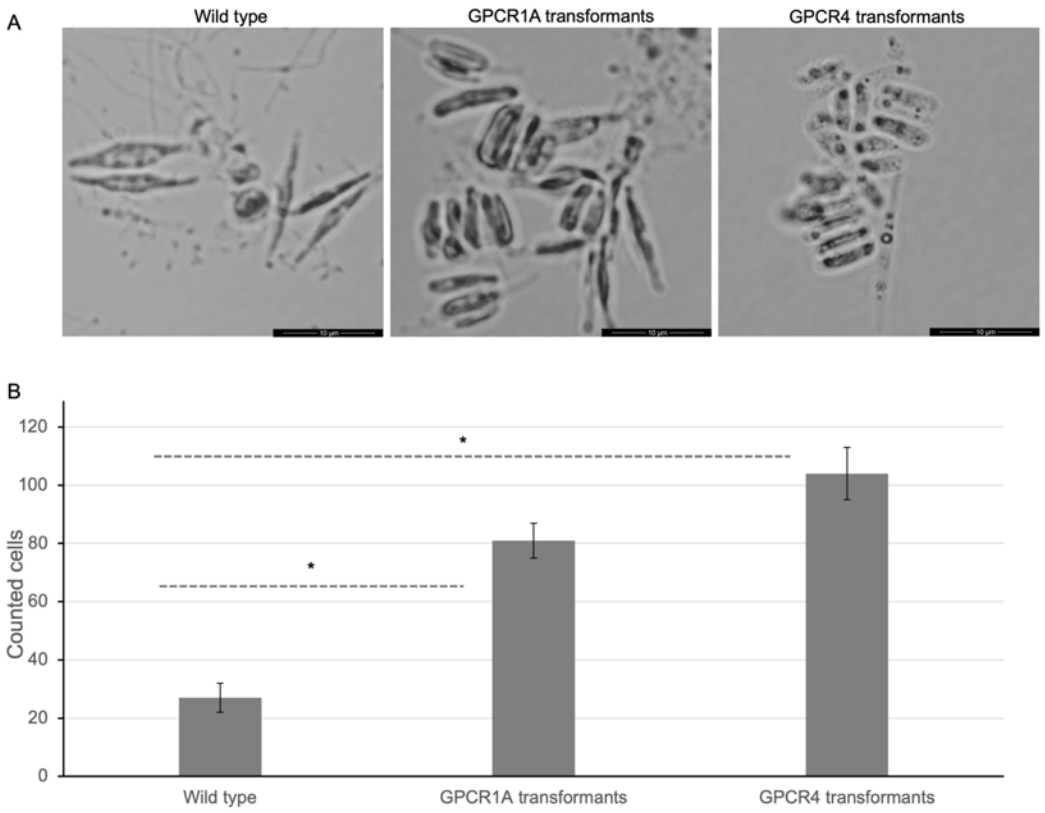

Fig. S6. Surface colonization of the wild type and the two transformants on glass slides over 72 hours, related to Figures 3 and 4. (A) Brightfield microscopy image of the cells on glass slides. Oval cells were observed as the dominant form in the population of the two transformants with the 100X objective lens using oil immersion. **(B)** More cells of transformants were attached to the glass slides in comparison with the wild type. Cells were counted based on a total of 9 fields of view for each glass slide. Detailed information on surface colonization experiments is present in the Methods section. The symbol (*) indicates a significant difference between the two groups ($p=0.032$ for comparison between the wild type and GPCR1A transformants, and $p=0.039$ for comparison between the wild type and GPCR4 transformants, respectively); however, there is no significant difference between GPCR1A transformants and GPCR4 transformants ($p=0.103$).

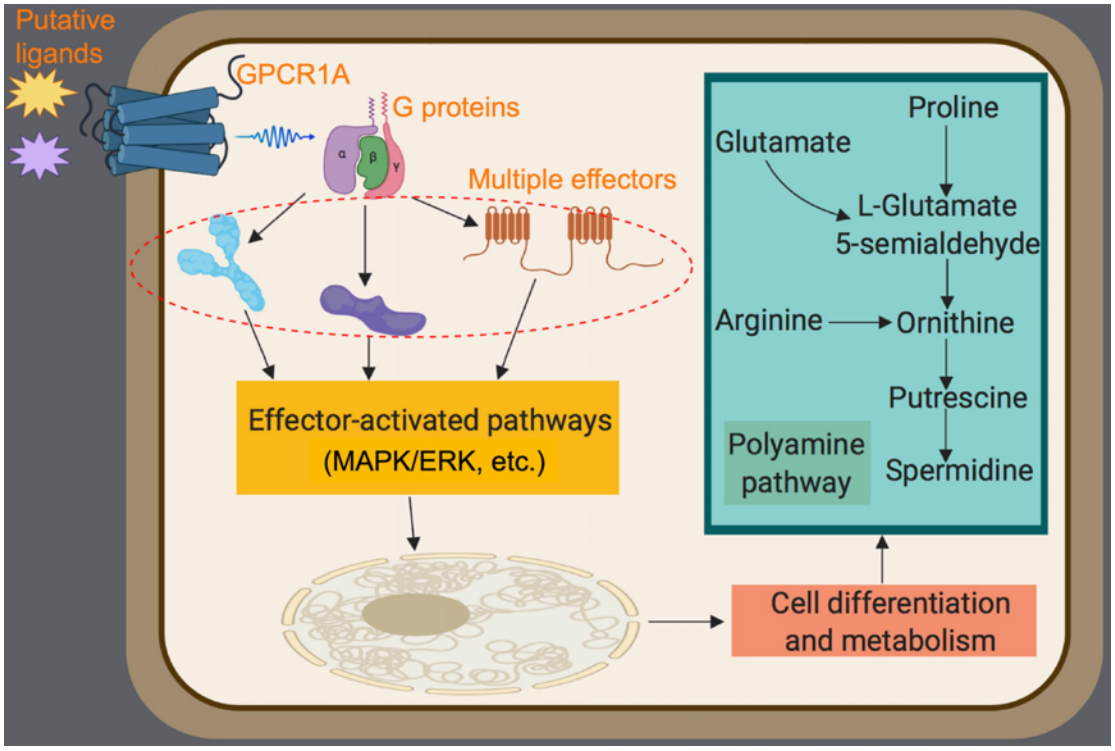

Figure S7. An overview of key putative signaling and metabolic pathways affected in GPCR1A transformants, related to Figure 6. The illustration of major signaling network elements was derived from Figure 6 based on network reconstruction and whole transcriptome analysis. The environmental signals (putative ligands) can bind to GPCR1A, and the associated G-proteins induce the downstream effector-activated pathways (e.g., MAPK/ERK). The G-protein (consisting of α, β, and γ subunits) is separated in the illustration from GPCR1A for the visualization of its activation by the receptor moiety (the drawing does not reflect the actual localization of the G proteins, which are otherwise closely associated with the receptor). The figure also highlights the GPCR-mediated activation of the polyamine synthesis pathway as polyamines play an important role in silica precipitation for the formation of siliceous shells of diatoms. MAPK/ERK: mitogen-activated protein kinase or extracellular signal-regulated kinase.

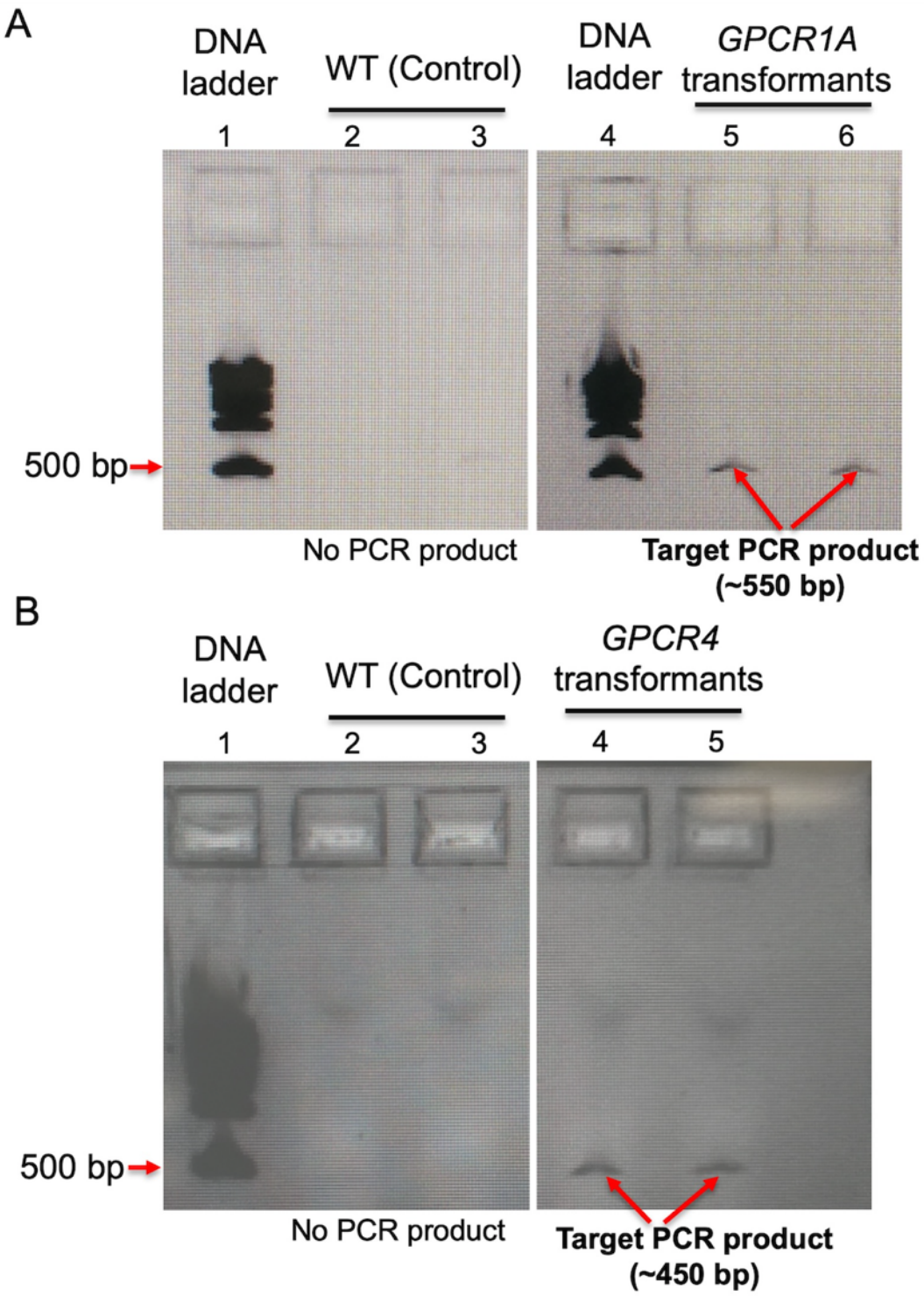

Fig. S8. PCR verification of *GPCR* transformants based on genomic DNA, related to Figures 3 and 4. (A) Primers (Forward, 5'-CACAAACCGAACAGCCCTAC-3'; Reverse, 5'-TCGAGCTTCACAACCTGTCC-3') were used to amplify DNA fragment across

the nitrate reductase promoter and GPCR1A gene to verify the positive transformation of the synthetic DNA construct into *P. tricornutum* cells; **(B)** Primers (Forward, 5'-CACAAACCGAACAGCCCTAC-3'; Reverse, 5'-CAGTGACGTTGCGACAATCC-3') were used to amplify DNA fragment across the nitrate reductase promoter and GPCR4 gene to verify the positive transformation of the synthetic DNA construct into *P. tricornutum* cells.